The developing infant gut microbiota: mathematical predictions of the effects of oligosaccharides

Versluis, D.M.

Chapter 5

Multiscale modelling of post-antibiotic recovery in the newborn infant gut microbiota

Authors
David M. Versluis[a], Ellen Looijesteijn[b], Jan M. W. Geurts[b],
Roeland M. H. Merks[a,c]
Affiliations
[a] Leiden University, Institute of Biology, Leiden, The Netherlands
[b] FrieslandCampina, Amersfoort, the Netherlands
[c] Leiden University, Mathematical Institute, Leiden, The Netherlands

In preparation

Abstract

The infant gut microbiota is a dynamic ecosystem that is crucial for infant health. The microbiota can be disturbed by antibiotics, infection, or diarrhoea. In this chapter we use a computational model to predict and explain the effects of such disturbances on the infant gut microbiota. We focus in particular on antibiotics, though we expect that our results generalize to other disturbances as well. Antibiotics decrease the abundance of pathogenic bacteria. However, antibiotics typically also cause an increase in potentially harmful Enterobacteriaceae, a decrease in beneficial *Bifidobacterium* bacteria, and an overall decrease in diversity. Many factors, such as antibiotic resistance and inflammation-induced host metabolites may be involved, but it is unclear which factors are most important. We examine in particular whether bacterial dynamics can explain, at least in part, the observed effects of disturbances, and if prebiotics can improve the resilience of the gut microbiota. We investigated these factors using a computational model that describes the metabolism and ecology of the infant gut microbiota. The model predicts that strong disturbances in the gut microbiota due to simulated antibiotics exposure lead to a decrease in the temporal stability of the microbiota, which is reflected by changes in the bacterial composition and lowering of the microbial diversity. The model only reproduces the increase in Enterobacteriaceae and decrease in *Bifidobacterium* observed *in vivo* when disturbances of intermediate strength are applied to the microbiota. The model predicts that disturbances impact acid production, particularly butyrate. Supplementation with 2'-fucosyllactose or galacto-oligosacharides, common prebiotics, make the model microbiota recover more consistently after antibiotic exposure. The model still predicts a disturbed acid production with these prebiotics, which may have health impacts. Altogether, the model can function as a framework for further investigations into the potential effects of different disturbances and their interaction with nutrition.

5.1 Introduction

The infant gut microbiota, which is important for normal growth and development [180], can be disturbed by antibiotics [257], bacterial and viral infections [258], or diarrhoea [259]. These kinds of disturbances have a complex effect on the composition and metabolic activity of the microbiota, which potentially has an impact on health. In this study we use a computational multiscale model to generate predictions of how antibiotics treatment disturbs the infant gut microbiota and affects microbiota composition and metabolic activity. We expect that many of our predictions will generalize to other disturbances as well, like bacterial and viral infections and diarrhoea. Disturbances of the microbiota by antibiotics are common in infants [257]. Antibiotics are administered to infants both preventatively and to treat bacterial infections [58]. Ampicillin and gentamicin are the most commonly used for infants, but many others are in use [257]. Antibiotics in infants are specifically associated with negative health outcomes such as asthma [260], wheezing [261] and gastro-intestinal disorders [262]. These health effects have been linked to differences in the composition and metabolism of the gut microbiota caused by the antibiotics [260, 261, 262] and have been described both *in vivo* and *in vitro*. Both *in vivo* and *in vitro* antibiotic treatment impacts the composition of the microbiota by increasing the relative abundance of Enterobacteriaceae, such as *E. coli* [263, 57, 59, 60, 58, 264, 52], decreases the abundance of *Bifidobacterium* spp. [263, 57, 58, 264, 52], and lowers the overall diversity [57, 58]. Breastfeeding seems to mitigate some of these negative effects, probably through its positive effect on the abundance of *Bifidobacterium*[265]. Some infants consume infant formula with *Bifidobacterium*-stimulating prebiotic oligosaccharides [71]. These infants may also be protected to some extent.

Mechanistic insights in how antibiotics impact the gut microbiota are sparse. Some bacterial species are more resistant to antibiotics than others [266], however, antibiotic resistance is generally low in the infant gut even after treatment [264]. It has also been hypothesized that the release of oxygen or nitrate by the gut wall may lead to an increase in the facultatively anaerobic Enterobacteriaceae over the strictly anaerobic *Bifidobacterium* [267, 268, 269]. However, the increase in Enterobacteriaceae has been replicated in an *in vitro* model that did not include a gut wall [263], suggesting that oxygen and nitrate input from the gut wall are not totally explanatory. With our model, we examined whether the observed effects can, at least partially, be explained by metabolic interactions between bacteria itself. Specifically,

we aimed to answer the following questions:
(1) Can the consequences of antibiotics exposure on the infant gut microbiota described *in vivo* be reproduced in our multiscale model on the basis of metabolic interactions between bacteria alone?
(2) How do model results depend on the strength of disturbance?
(3) Can the model predict potential health effects caused by an antibiotic disturbance?
(4) What role can the prebiotic oligosaccharides 2'-fucosyllactose (2'-FL) and galacto-oligosacharide (GOS) play in recovery from an antibiotic disturbance?

To answer these questions we used and further developed an existing multiscale computational model [122, 103, 229]. An earlier version of this model had already been used to study the effect of a diarrhea-like disruption of the microbiota, but focused on the disturbed spatial structure, not on a decline in population [122]. This version of the model predicted that increased flow through the gut decreases metabolic diversity by making cross-feeding more difficult. This may explain the decreased microbial diversity often observed in patients with diarrhea [122]. As an extension to the model, we will focus here on bacterial population dynamics and model how antibiotics may influence spatial separation and cross-feeding. For this we use a more concretely defined infant gut microbiota, with genome-scale metabolic models (GEMs) specific to infant bacteria, and detailed modelling of prebiotic metabolism, as reported in our previous study [229] and chapter 5. We disturb the microbiota by killing a large part of the population on days 8 and 9, and monitor the recovery both for simulated infants that have had no prebiotics in their nutrition, and those that have had prebiotics in their nutrition since birth.

Briefly, we show that:
(1) The model can reproduce the effects of an antibiotic disturbance observed *in vivo*: an increase of the Enterobacteriaceae population, the decrease of *Bifidobacterium*, and lower diversity, but the first two effects are only reproduced at an intermediate strength of disturbance.
(2) The model predicts that antibiotics may negatively affect the production of organic acids in general in the short-term, and decrease butyrate production specifically in the longer-term.
(3) The model predicts that ongoing supplementation with prebiotics, before, during, and after antibiotic treatment, leads to a consistently *Bifidobacterium*-dominated mi-

crobiota, with smaller *Bacteroides* and *E. coli* populations, and that infants who are given prebiotic supplementation return to this composition more consistently after antibiotic treatment.

5.2 Results

5.2.1 Stronger disturbances kill more bacteria but impact relative abundances in different ways

To investigate the effect of different strengths of antibiotics-related microbiota disruption, including the complex spatial and temporal bacterial interactions, we use a multiscale computational model based on our earlier models [122, 103]. The spatial component of the model consists of a regular square lattice of 225×8 (Fig. 5.1A), where each lattice site can contain a single population of a single species, as well as any number of metabolites in any concentration. Each species has its own GEM, selected from an existing database [101]. We use a set of 21 species derived from *in vivo* data [3] (Table 5.1, methods section 'Species composition'). We simulate the model in timesteps, each of which represents three minutes of simulated time. At each timestep, the model uses the nutrients and metabolites available in each lattice site, and the GEM of each population, to calculate metabolism per population using flux balance analysis (FBA). For each population, FBA returns a set of inputs and outputs, which we apply to the local environment as well as a growth rate, which we apply to the local population (Fig. 5.1A-1). Populations that grow large enough can spread to neighbouring lattice sites. There is also a small probability for each population to be removed from the system after each timestep, to represent natural turnover of populations. The model is initialised with a probability for each lattice site to acquire a population of a random species. Every timestep, there is small chance for each empty lattice site to acquire a new population of a random species, to represent the input of bacteria from the environment. Populations diffuse throughout the lattice (Fig. 5.1A-2). Nutrients and metabolites diffuse (Fig. 5.1A-3) and advect towards the rightmost edge of the system (Fig. 5.1A-4), where they are removed. Every 60 timesteps 211 µmol of lactose is placed distributed over the most proximal columns, and 0.5 µmol of mucin is placed at the bottom-most row of the lattice every timestep. We run the model for 20160 timesteps, equivalent to a simulated 42 days.

Over time, a complex microbiota and metabolic ecology forms (Fig. 5.1B).

Table 5.1: Species and subspecies included in the model. Color indicates group and color used in figures.

Name	Phylum
Bifidobacterium longum ssp. *infantis*	Actinomycetota
Bifidobacterium breve	Actinomycetota
Bifidobacterium bifidum	Actinomycetota
Collinsella aerofaciens	Actinomycetota
Cutibacterium acnes	Actinomycetota
Eggerthella sp. *YY7918*	Actinomycetota
Rothia mucilaginosa	Actinomycetota
Anaerobutyricum hallii	Bacillota
Clostridium butyricum	Bacillota
Roseburia inulinivorans	Bacillota
Enterococcus faecalis	Bacillota
Gemella morbillorum	Bacillota
Lactobacillus gasseri	Bacillota
Ruminococcus gnavus	Bacillota
Staphylococcus epidermidis	Bacillota
Streptococcus oralis	Bacillota
Veillonella dispar	Bacillota
Bacteroides vulgatus	Bacteroidota
Parabacteroides distasonis	Bacteroidota
Escherichia coli SE11	Pseudomonadota
Haemophilus parainfluenzae	Pseudomonadota

In our model we represent the effect of antibiotics treatment by increasing the population death probability on days 8 and 9 of the model, to mimic a typical duration for an antibiotic disturbance [57]. This causes the population size of all species to decrease greatly (Fig. 5.1C). Because nutrient input and bacterial metabolism continues, this leads to a unique new environment.

Our model is stochastic, which allows it to reach a wide variety of outcomes in terms of the abundances of species and metabolites, even when the parameters are constant. This spectrum of outcomes is similar to that of the *in vivo* infant gut microbiota [103, 31]. However, stochastic behaviour necessitates the comparison of bacterial populations of separate control and test simulations. We performed sets of 30 simulations without any disturbance, and with four levels of severity of disturbance. Each simulation had a unique random seed, for a total of 150 unique random

seeds. The severity of disturbances ranged from an increased death probability for all populations by a factor of 1.75 to a factor of 2.5. We first quantified how the different death probabilities impacted the absolute abundance immediately after the disturbance period ended at the end of day 9 (Fig. 5.1D). Disturbances caused much of the population to be killed, and more severe disturbances killed more of the population, ranging from 81% to 99%. We will use these percentages to indicate the disturbance strength from here on. When 99% of the population was killed, the system was effectively reinitialised in many simulations, as the model only maintained the concentration of metabolites and nutrients.

We next analysed the relative abundances of bacterial groups in the control and antibiotics-exposed simulations. To make comparisons easier, and allow focus on large-scale differences, we grouped the three *Bifidobacterium* species and the three butyrate producers together as separate groups, since they have similar metabolisms and ecological roles [90, 91, 20]. We also merged the 13 other species that remained at very low abundance in all simulations (indicated in Table 5.1). Where relevant, we also performed analysis with all species separately.

As shown in Fig. 5.1E, the model predicts a microbiota on day 42 composed mostly of *Bacteroides vulgatus*, *Bifidobacterium* spp., and *Escherichia coli*, in line with the most common genera in infants at this age [3, 31]. The antibiotics exposure that killed 81% of the total population had little effect, whereas an exposure leading to a reduction of 91% lowered the abundance of *Bifidobacterium* compared to the undisturbed simulations (p=0.001) and increased the abundance of *E.coli* (p=0.019) significantly, in agreement with reported *in vivo* observations [57, 58]. Interestingly, the microbiota composition changed differently for disturbances killing more than 91%. In these situations *Bifidobacterium* remained approximately at the level of the control situation. When the severity of the antibiotics disturbance was further increased to a 99% reduction of bacterial abundance, the relative abundance of *E. coli* was reduced (p=0.011), while butyrate producers became more abundant (p=0.002). These results show how the various degrees of antibiotic disturbances impact the model in a complex and non-linear way. To further analyse these effects we investigated the changes in more detail over time.

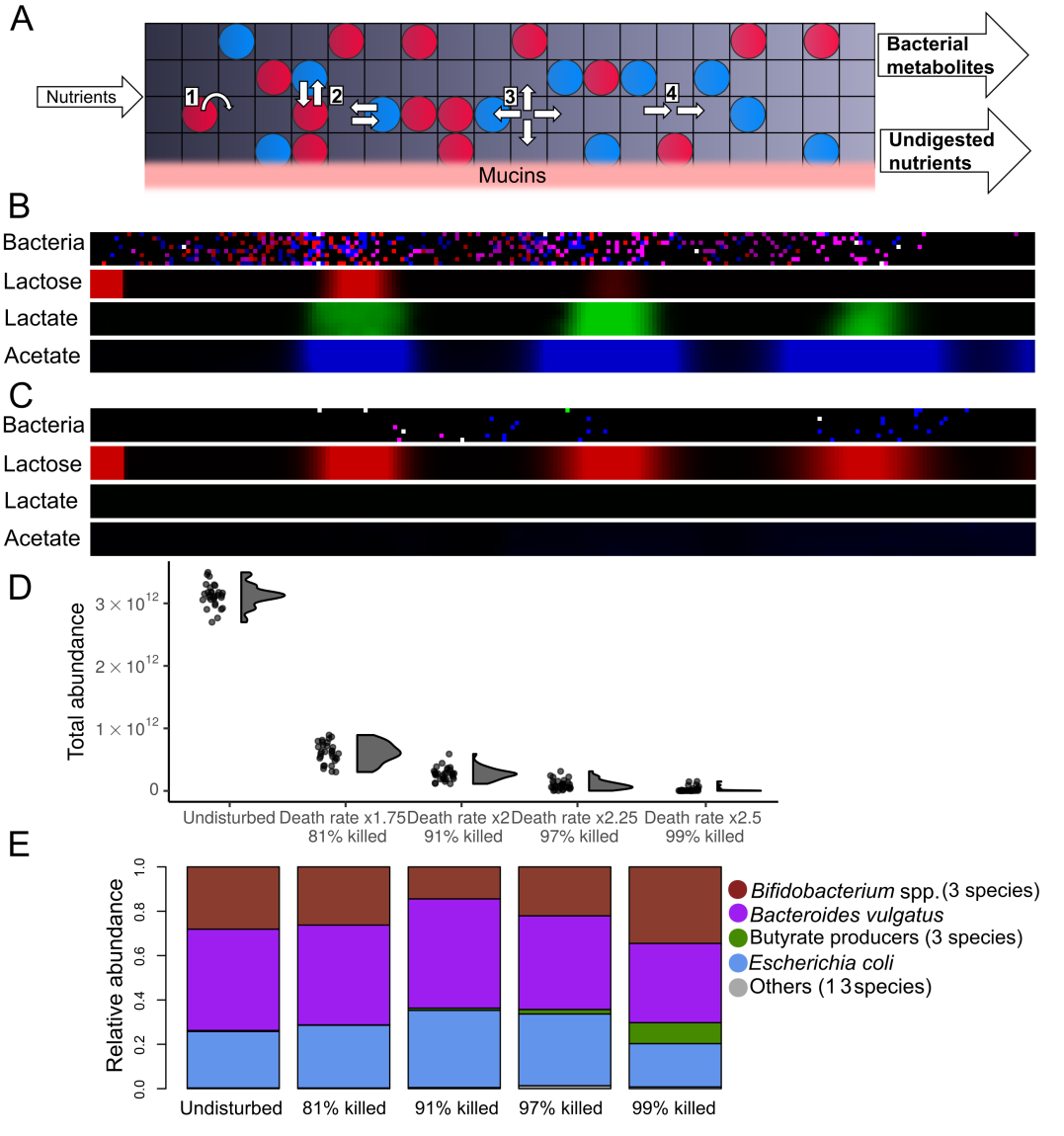

Figure 5.1: Model predicts complex effect of disturbance on relative bacterial abundances

(A) Schematic of the model. Circles represent bacterial populations. Numbers indicate processes in the model: (1) Bacterial growth and division (2) Bacterial diffusion (3) Metabolic diffusion (4) Metabolic advection **(B,C)** Screenshot of the model at the start of day 10, displaying the bacterial layer and three of the metabolic layers, in (B) an undisturbed simulation (C) a simulation with a modelled disturbance **(D)** Total bacterial abundance immediately after the disturbance (at the start of day 10) per condition. n=30 per condition. **(E)** Relative abundance of bacterial species on day 42 without disturbance or with a disturbance on the simulated day 8 and 9, n=30 per condition

5.2.2 Disturbances disrupt species composition and decrease diversity; correlation to pre-exposure populations is lost

Interestingly, we observed that in the conditions that killed 81% or 97% the relative abundance of all bacterial groups did not change. Did the antibiotics disturbances in these cases still have an effect on the microbiota, even when there was no difference in relative abundance? To answer this question we examined what impact each antibiotics disturbance had, by calculating the Bray-Curtis dissimilarity between abundances, as is commonly performed on microbial abundance data [20, 4]

We visualised the dissimilarity between the grouped relative abundances at the endpoint of the undisturbed simulations and at each timepoint in each set of simulations (Fig. 5.2 A&B and Fig. S1) and observed that all sets of simulations moved towards the same distribution (Fig. 5.2 A&B and Fig. S1), but stronger disturbances appeared to remain more distant from the undisturbed simulations. This was also the case when we analysed the dissimilarity without grouping bacterial abundances (Fig. S2), or when we analysed the Euclidean distance instead of the Bray-Curtis Dissimilarity (Fig. S3&S4, methods section 'Analysis'). To quantify the difference between disturbed and undisturbed simulations, we calculated the Bray-Curtis dissimilarity on day 42 between each simulation and the mean of the undisturbed simulations. ANOVA analysis revealed a significant effect of the disturbances on the dissimilarity ($p<0.0001$). Each disturbance that killed more than 81% was further away from the baseline than the disturbance that killed 81% ($p<0.001$ for all,Fig. 5.2C). Even the 97% condition, which did not differ from the undisturbed condition in mean bacterial abundances per group, did differ in this metric. When we did not group the species, the differences were still significant, but less so ($p=0.04$,$p=0.008$ and $p<0.001$, Fig. S5A). We also examined the Bray-Curtis dissimilarity between each pair of simulations within each condition, and found that conditions with a stronger disturbance had a higher dissimilarity ($p=0.005$ for the 81% disturbance, $p<0.001$ for all others, Fig. S5B). This shows that the disturbances not only cause a higher dissimilarity from a non-disturbed baseline, but also cause a wider variation of outcomes. We concluded that all disturbances influence the microbiota, and that disturbance strength matters for the effect.

We next examined whether the disturbances also affected species diversity, as is often observed *in vivo*. We calculated Shannon diversity, a common metric for bacterial diversity [57, 58], for each simulation to give a metric for how the distribu-

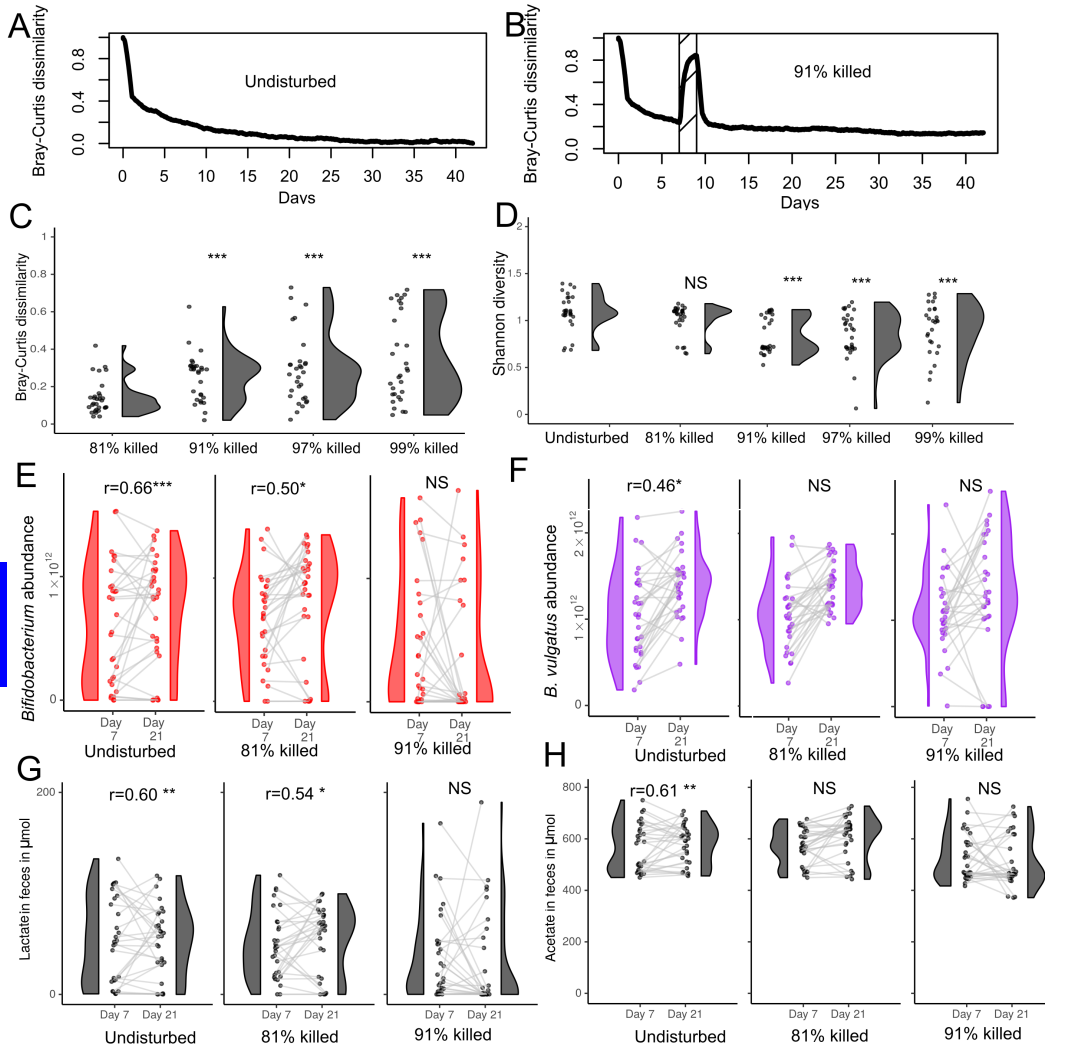

Figure 5.2: Stronger disturbances cause a larger distance from baseline, lower diversity, and disturb temporal stability more

(A,B) Bray-Curtis dissimilarity between the mean abundance at every timestep of the major bacterial groups (Table 5.1) the undisturbed condition and the condition where 91% were killed in Fig. 1D, compared to the mean abundance of the undisturbed simulations at day 42 (timestep 20160). Striped area indicates the duration of the disturbance. **(C)** Bray-Curtis dissimilarity by simulation between the mean relative abundance grouped by group, as in table 5.1, at day 42 (timestep 20160), compared to the mean relative abundance grouped in the same way of the undisturbed simulation at day 42. n = 30 per condition **(D)** Shannon diversity for all simulations in each condition at day 42 (timestep 20160). **(E,F)** Absolute abundance of (E) *Bifidobacterium* spp. (F) *B. vulgatus* per simulation at the end of day 7 and day 21 for the first three conditions of Fig. 5.1E. Points from the same simulations are connected with a line. Spearman correlation between day 7 and day 21 indicated where significant. n=30 per condition **(G,H)** Quantity of (G) lactate (H) acetate per simulation at the end of day 7 and day 21 for the first three conditions of Fig. 5.1E. Points from the same simulations are connected with a line. Spearman correlation with Bonferroni correction between day 7 and day 21 indicated where significant. n=30 per condition. NS: Not significant, *: $p<0.05$, **:$p<0.01$, ***:$p<0.001$

tion of diversity differs. We calculated the Shannon diversity using the abundance of each individual species in each simulation, as in [57, 58]. An ANOVA analysis found a significant effect of disturbances on the diversity ($p<0.0001$). With pairwise comparisons we found that only the simulations with disturbances where more than than 81% was killed were significantly less diverse than undisturbed simulations ($p<0.001$), but the simulations also varied greatly in their diversity (Fig. 5.2D). In all tested conditions many simulations did reach a diversity similar to the typical undisturbed situation (Fig. 5.2D). Richness was equally high in all these simulations on day 42, as all species were present in all simulations. When we removed species with an abundance below 10^{10} from the data, species richness was between 2 and 5 for each simulation on day 42 (Fig. S6A). An ANOVA analysis showed a significant effect of disturbances ($p=0.005$), but in pairwise comparisons only the set of simulations that killed 99% was significantly less rich ($p=0.0001$). When we removed species with an abundance below 10^{10} from the data, diversity remained similar (Fig. S6B). We also calculated Sheldon's index, which is a measure of evenness. We found that it matched closely with the diversity when the less abundant species were included (Fig. S6C). However, when we excluded the less abundant species, only the condition that killed 99% had less evenness than the baseline ($p<0.001$, Fig. S6D). We conclude that a reduced evenness may explain the lower diversity in the disturbed conditions, but that reduced evenness alone does not explain the decreased diversity when we remove less abundant species. We further examined the distribution of outcomes with a principal component analysis on the abundance by genus (Fig. S6E), which showed a great variability between simulations and conditions. It also showed that *Bifidobacterium*, *Bacteroides* and *Escherichia* were the major drivers of differences in abundance. Thus our stochastic model predicts that after a disturbance in some infants the microbiota either maintains or recovers its diversity completely, while in others it loses some of its diversity and evenness. The model predicts that this leads to a wide variety of outcomes.

We proceeded to examine how disturbances may lead to new outcomes, and whether we can identify a factor that functions as the 'memory' of the system: a factor that persists throughout the disturbance and can be used to predict how a microbiota responds to a disturbance. We first examined whether we could link the bacterial community composition before the disturbance to that after the disturbance. To do so we calculated the Spearman correlation within the same simulations between day 7 and day 21 for the total abundance of each major group. We did so

separately for each bacterial group, so that we have a p and r value for each bacterial group for each condition. We observed that in the undisturbed simulations a correlation between abundance on day 7 and day 21 existed for *Bifidobacterium* and for *B. vulgatus* (Fig. 5.2E&F, r=0.66 & r=0.46, p<0.001& p=0.04 including Bonferroni correction). These correlations were not present with any disturbance for *B. vulgatus*, nor were they present with at least a disturbance that killed 91% for *Bifidobacterium*. *E. coli* never had a significant correlation (Fig. S7). We conclude that bacterial abundances before a disturbance are not indicative for the abundances after the disturbance. We next examined whether the quantity of nutrients or metabolites might serve as 'memory' for the system, by also examining their correlation within the same simulations between day 7 and day 21. We measured the amount of acetate and lactate leaving the system per 60 timesteps. Acetate and lactate were correlated in the undisturbed condition (r=0.61 & r=0.60, p=0.002&p=0.003, Fig. 5.2 G&H). Interestingly, lactate remained correlated even with the disturbance that killed 81% (r= 0.54, p=0.01), though the correlation was weaker than in the undisturbed condition. This indicates that the system does have a 'memory' for the excretion of lactate that persists through a disturbance. We also tested the correlation for lactose, mucin, and butyrate, but these did not even correlate significantly in the undisturbed condition (p>0.05). Oxygen was no longer present in any simulation at the start of the disturbance. We conclude that there is no temporal correlation between bacterial abundances or metabolite concentrations in the system with a disturbance that kills at least 91%, indicating that it does not have a 'memory'.

5.2.3 Disturbances disrupt acid production and cross-feeding

We previously noted that the model predicted a decrease in *Bifidobacterium* abundance and increase in *E. coli* abundance with the disturbance that killed 91% of the population. *Bifidobacterium* is positively associated with infant health due to, among other factors, its production of acids [19, 18]. We next investigated what effects of a disturbance the model predicts for acids produced by the bacteria. We used the condition that killed 91% of the population, as this provided the closest match to *in vivo* data [57].

We examined: (1) organic acids in general, which provide resistance to pathogens[18], (2) the short-chain fatty acid butyrate, which is associated with a reduction in allergies [20] and (3) lactate, which is an important acidifier and cross-feeding substrate

[74]. For each aspect we compared the simulation where 91 % was killed with the undisturbed, control simulations. Fig. 5.3 shows the results of these analysis. We found that there was significantly less total organic acid, butyrate, and lactate in feces 480 timesteps (one simulated day) after the antibiotic disturbance ($p<0.001$, $p=0.03$,$p<0.001$ Fig. 3A-F). Though the mean amount of lactate present was also lower before the disturbance due to stochasticity (Fig. 5.3E), there was no significant difference immediately before the disturbance (timestep 3360, $p=0.445$). We further examined why there was less lactate after the disturbance, as lactate is both produced and consumed in the infant gut and in our model [74, 103]. We found that there was less lactate in the feces due to a reduced production of lactate ($p<0.001$), not an increased consumption. In fact, consumption also decreased ($p<0.001$, Fig. 3G&H). We concluded that there are many potential impacts on metabolites that are relevant for infant health. These effects may explain some of the health effects observed in infants *in vivo* [260, 261, 262].

5.2.4 Prebiotic-fed microbiotas recover more consistently from a disturbance

The simulations predicted that simulated antibiotic disturbances affect many aspects of the infant gut microbiota, including various metabolites related to infant health. We next asked whether the resilience of the system could be improved in order to reverse these effects. *In vivo*, breastfeeding protects against some of the negative effects of antibiotic treatment, which is thought to be caused by the presence of prebiotic oligosaccharides in human milk [265]. These prebiotic oligosaccharides stimulate, amongst others, *Bifidobacterium* [63, 64]. We asked if and how prebiotics, in particular the prebiotic oligosaccharides 2'-fucosyllactose (2'-FL) and galacto-oligosaccharides (GOS), could affect the recovery after disturbance in the model. 2'-FL is the most abundant oligosaccharide in most human milk samples [66], and GOS is commonly used in infant formula [71]. We simulated three conditions. In each condition we added additional sugars to the base amount of 211 µmol of lactose: (1) Addition of 211 µmol 2'-FL (2)Addition of 42.2 µmol 2'-FL and 168.8 µmol GOS, a ratio as used in infant formula, (3) Addition of 211 µmol lactose, as a control condition. The third condition allowed us to discern between effects from the specific sugars we added, and an effect from the total amount of sugar present. We used the antibiotics disturbance that killed 91% of the population in earlier simulations, as it

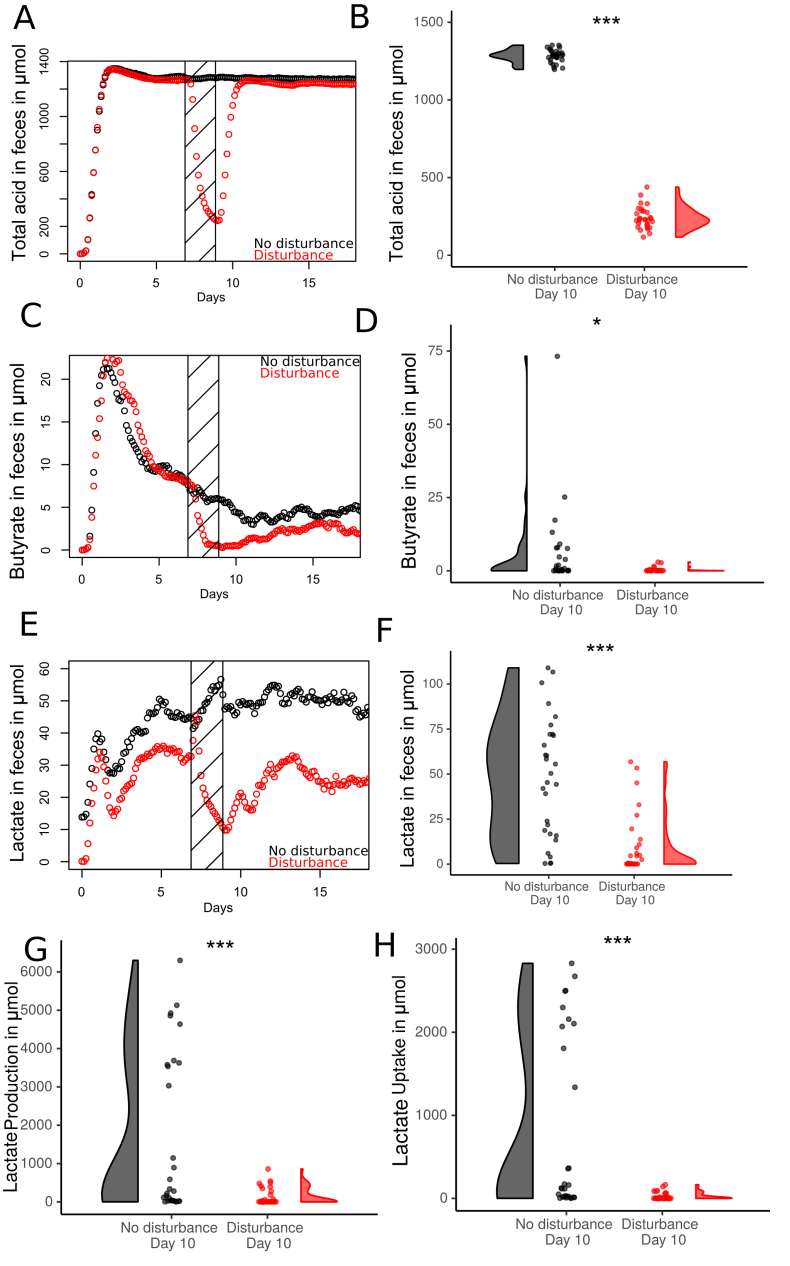

Figure 5.3: Disturbances influence metabolites and metabolism
(A,C,E) (A) Total acid, (C) butyrate, or (E) lactate leaving the system per 60 timesteps in the model with no disturbance (black) and the model with 91% killed disturbance (red). Striped area indicates the duration of the disturbance, n=30. **(B,D,F)** (B) Total acid, (D) butyrate, or (F) lactate leaving the system from timestep 4320 to 4360, immediately after the end of the disturbance, compared to the same steps in the undisturbed simulations, n=30. **(G)** Total lactate production per simulations from timestep 4320 to 4360 , immediately after the end of the disturbance, compared to the same steps in the undisturbed simulations, n=30. **(H)** Total lactate consumption per simulations from timestep 4320 to 4360, immediately after the end of the disturbance, compared to the same steps in the undisturbed simulations, n=30. NS: Not significant, *: $p<0.05$, **:$p<0.01$, ***:$p<0.001$

produced the best match with *in vivo* data [57]. Fig. S8 shows that the combined addition of 2'-FL and GOS reduced the Bray-Curtis dissimilarity and Euclidean distance from the baseline on day 42 compared to the condition that killed 91% that did not have additional sugar (Fig. S8D&E, $p<0.001$). However, the control condition, where we only added lactose, also reduced the distance ($p=0.013$). Thus, we could not conclude that the prebiotics had an effect. The reduced Bray-Curtis dissimilarity may have been caused by a higher total bacterial abundance alone. The post-disturbance populations were indeed much larger than the post-disturbance populations in the simulations without added sugars (Fig. S8F, Fig. 5.1D).

To control for an increased total bacterial abundance, we next performed additional simulations where the total amount of sugar was kept the same as in the simulations of Fig. 5.1. We used two conditions: (1) 105.5 µmol of lactose replaced with 2'-FL (indicated with 1/2 2'-FL in fig. 5.4) (2) 21 µmol of lactose replaced with 2'-FL and 84.5 µmol of lactose replaced with GOS (indicated with 1/2 2'-FL&GOS in Fig. 5.4). We performed these simulations both without a disturbance and with a disturbance that killed 91%. The results are displayed in Fig. 5.4. Either condition led to a total bacterial abundance comparable to the abundance without prebiotics (Fig. 5.4A). Compared to the simulations with the same disturbance, but without prebiotics, there was much more *Bifidobacterium* (Fig. 5.4B& Fig. 5.1, $p<0.001$). There were no significant differences in relative abundance between the disturbed and undisturbed simulations (Fig. 5.4B, $p>0.05$). We calculated the dissimilarity between each prebiotic condition with and without a disturbance. There was a lower dissimilarity, compared to the simulations without prebiotics (Fig. 5.4C, $p=0.001$ for 2'-FL, $p<0.001$ for 2'-FL+GOS). With either prebiotic conditions there was also no reduction in diversity due to the disturbance (Fig. 5.4D, $p>0.05$). This indicates that in the model the prebiotics-influenced microbiota was more resilient to a disturbance.

We also analysed the effects on total acids, butyrate, and lactate, as we did for the simulations without prebiotics (Fig. 5.4E-J). Total acids were disturbed in both conditions on day 10 ($p<0.001$), but butyrate was only disturbed in the condition with only 2'-FL ($p<0.001$). Nonetheless, butyrate was much more abundant even with a disturbance in the condition with 2'-FL, compared to any other condition ($p<0.001$). Lactate was increased in the simulations with both 2'-FL and GOS ($p<0.001$), but not with 2'-FL alone. In conclusion, the model predicted that supplementation with prebiotics led to a more consistent return to baseline after disturbance in the model, but metabolites, particularly total acids, and total bacterial abundance were still affected.

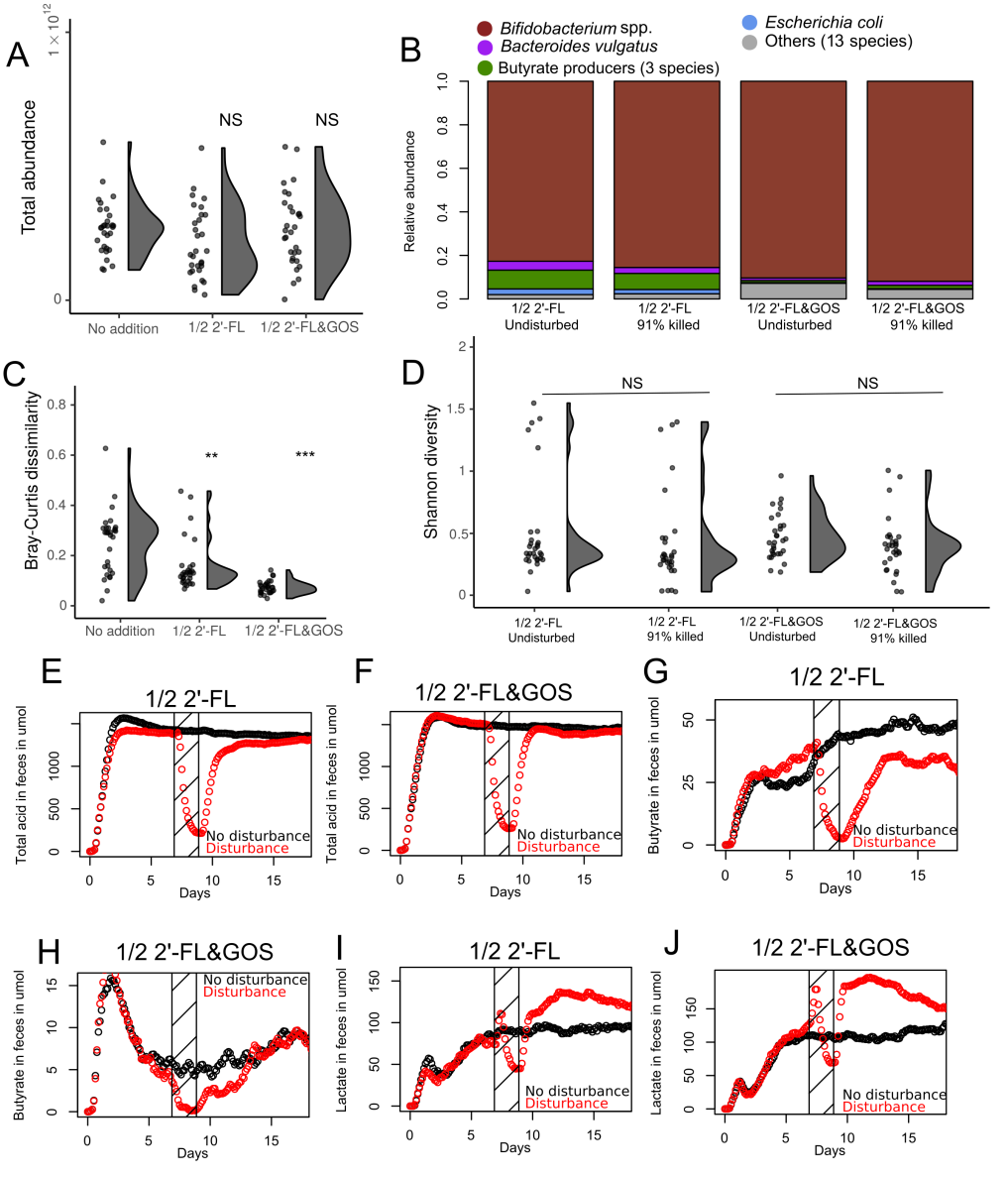

Figure 5.4: Prebiotics shape a more resilient microbiota
For all figures: '1/2 2'-FL' is 105.5 µmol of lactose replaced with 2'-FL, '1/2 2'-FL&GOS' is 21 µmol of lactose replaced with 2'-FL and 84.5 µmol of lactose replaced with GOS. n=30 per condition. NS: Not significant, *: $p<0.05$, **:$p<0.01$, ***:$p<0.001$ **(A)** Total bacterial abundance at the start of day 10 per condition in the disturbed simulations. **(B)** Relative abundance of bacterial species on day 42 without disturbance or with a disturbance on the simulated day 8 and 9. **(C)** Bray-Curtis dissimilarity by simulation between the mean relative abundance on day 42 (timestep 20160) of the simulations of A, grouped as in table 5.1, compared to undisturbed simulations with the same nutrition at day 42. **(D)** Shannon diversity for all simulations in each condition of B. **(E-J)** Total acid, butyrate, or lactate leaving the system per 60 timesteps in the model with no disturbance (black) and the model with 91% killed (red). Striped area indicates the duration of the disturbance.

5.3 Discussion

In short, the simulations predicted that (1) an antibiotic disturbance that kills 91% of bacteria increases the abundance of Enterobacteriaceae and decreases the abundance *Bifidobacterium*, (2) any disturbance that kills at least 91% of bacteria decreases diversity, (3) a disturbance that kills 91% of bacteria may reduce production of acids, and in particular butyrate, which may have health effects, (4) prebiotics may create and sustain a more resilient microbiota that returns to the same state more consistently, but such a microbiota is still sensitive to disturbance of acid production. We will address the relation between each of these major predictions and the available *in vitro* and *in vivo* data in turn, and suggest some further simulations and analyses that may provide more insight.

Firstly, a reduction in the abundance of *Bifidobacterium* and increase in the abundance of *E. coli* after antibiotics are widely reported [57, 58, 264, 52]. The model also predicts this, but only for the disturbance that kills 91% (Fig. 5.1E). We hypothesise that the disturbance that killed 91% increased the relative abundance of *E. coli* and decreased *Bifidobacterium* because it interrupts and delays succession. Early in the model simulations, there is a higher abundance of *E. coli* (Fig. S7). *E. coli* is typically replaced by other species, such as *Bifidobacterium*, at later timepoints of the model (Fig. 5.1E). This same succession takes place in infants [32, 31]. An interruption of this succession in our model may then lead to a relatively large share of Enterobacteriaceae remaining in the gut compared to controls of the same simulated age. A delay in succession, and so a longer *E. coli*-dominated phase, has also been hypothesised to explain some of the increased *E. coli* observed in infants *in vivo* after an antibiotic disturbance [55]. Whether the model also predicts that this mechanism is important can be tested by adding an antibiotic disturbance at different stages of succession. Disturbances could be added at either a very early *E. coli*-dominated stage or at a stable state with low *E. coli* abundance, which the model typically reaches after several simulated weeks. This testing would reveal whether the increase in *E. coli* in the model depended on the succession stage during which the disturbance was applied. We further hypothesise that in our model weaker disturbances do not disturb the microbiota sufficiently to alter the course of the succession. Heavier disturbances may cause the population to go extinct, which resets the system and does not preserve the relatively high *E. coli* abundance. This would essentially re-initialize the system, but without oxygen. A re-initialisation would explain the increased abundance of the

strictly anaerobic butyrate producers in the model with the disturbance that killed 99% (Fig. 5.1E). Interactions with the level of oxygen present in the gut could also be modelled. We expect oxygen to still be abundant in the infant gut if the disturbance occurs in the first days after birth [103], and the model has previously predicted that variation in oxygen explains much of the variation in succession timing observed in the infant gut microbiota [103].

Secondly, a lower microbial Shannon diversity due to antibiotics is widely reported in infants [57, 58, 270]. The model reproduced the lowered diversity due to antibiotics with every disturbance that killed at least 91% and did not include prebiotics (Fig. 5.2D). The reduced diversity due to a disturbance has also been linked to a reduced stability of the microbiota [270], which the model also predicted (Fig. 5.2E-H). We found that the reduced diversity could be attributed to a lower evenness, not to the complete extinction of species. However, when we eliminated less common species from the data the lowered diversity was maintained, while the lower evenness was not, indicating that a lower evenness does not fully explain the lower diversity.

On a metabolic level the model predicted a reduced acid output during and after disturbance (Fig. 5.3). Such a reduction in acidity due to antibiotics has not been reported in infants, but it has in adults and mice [271, 272]. The metabolic effect of 2'-FL and GOS supplementation on an infant gut microbiota disturbed by antibiotics has been previously studied in an *in vitro* system [263]. This *in vitro* model predicted a positive effect of 2'-FL on butyrate production, and a lowered SCFA output with antibiotics, confirming predictions of our model. However, the *in vitro* model also predicted an increase in lactate concentration due to antibiotics in the absence of 2'-FL and GOS [263], while our model predicted a decrease in lactate concentration in all conditions except those with 2'-FL. It is unclear why this discrepancy is present. Further analysis of lactate production and consumption in our model may reveal what factors are responsible for the incorrect prediction. The authors indicate that *Enterococcus*-driven lactate production may explain the increase in lactate that they observed in their *in vitro* model[263]. *Enterococcus* was included in our bacterial composition, but did not reach a high abundance. Further analysis of the metabolism of *Enterococcus* in our model may reveal where it differs from the *in vitro* model.

Further analysis and simulations could also be performed to reveal why prebiotics cause a more consistent recovery in the model. The prebiotics we used caused *Bifidobacterium* species to become dominant in the model (Fig. 5.4B), while without prebiotics *E. coli* and *Bacteroides vulgatus* were also abundant (Fig. 5.1E). This

effect is also commonly seen *in vivo* [53]. We hypothesise that this stimulation of *Bifidobacterium* over other species causes the microbiota to consistently return to the same *Bifidobacterium*-dominated baseline in the model. As *Bifidobacterium* is associated with improved infant health [18], this would be a positive outcome for the infant. Whether the stimulation of *Bifidobacterium* by prebiotics is the crucial factor in determining the consistency of our outcomes could be tested by repeating the simulations, but only adding the prebiotics after the antibiotic disturbance. We hypothesise that this will lead to a similarly *Bifidobacterium*-dominated microbiota in most simulations, regardless of composition before the disturbance.

More generally, various discrepancies exist between the model predictions and available *in vivo* data. Most importantly, only the disturbance that killed 91% decreased *Bifidobacterium* abundance and increased *E. coli* abundance in the model, and the other disturbances did not. We hypothesised that this happened because the succession away from *E. coli* was interrupted. It is unclear how much of the infant gut microbiota is killed during an antibiotic disturbance, but decreased *Bifidobacterium* and increased Enterobacteriaceae (which includes *E. coli*) abundance are commonly seen in the *in vivo* infant gut microbiota as an effect of antibiotics, and no link to disturbance strength has been reported [57, 59, 60, 58]. In addition, Enterobacteriaceae also become more abundant due to antibiotic treatment in adult humans and adult mice [268], where there is no succession to disrupt. There must be some further factor, unrelated to succession, that causes the increase in Enterobacteriaceae in antibiotic-treated adults. This factor may also cause the increase in Enterobacteriaceae to be much more consistent in infants than what we find. This factor could be a higher resistance of Enterobacteriaceae to antibiotics [266], or Enterobacteriaceae benefiting more than other bacteria from the inflammation-related release of oxygen and nitrate [268, 269]. Neither of these factors are currently included in the model, but they could be included in future versions. Modelling may allow us to explain which of these factors can explain the increase in Enterobacteriaceae observed *in vivo*.

Further simulations should also be performed to account for the possible effects of changes to parameters on the model predictions. In previous work (e.g. [103]) we found a large impact of several of the model parameters on the predictions, such as the amount of oxygen and the diffusion speed of metabolites. These factors may interact with an antibiotic disturbance. Disturbance could also be modelled in different ways in future extensions of the model. For example, injected antibiotics may

affect the gut microbiota from the gut wall, while antibiotics taken orally might have a stronger effect in the lumen. Each of these effects could be modelled to have spatially different effects in our model. In addition, our modelling of the disturbance as an increased death rate is a large simplification of the effect antibiotics have on the microbiota. Most antibiotics used in infants interfere with cell wall synthesis or ribosomal function, and so reduce growth, or make growth more energetically expensive [257]. In our model, this may be more appropriately considered as an altered biomass reaction, instead of an increased death rate. This may lead to more accurate predictions of the effect of antibiotics on microbial metabolism. Finally, additional model simulations with variation in the timing, quantity, and type of prebiotic oligosaccharides could provide more insight into the circumstances required for prebiotics to shape or restore the composition of the microbiota. In short, the presented work provides a starting points for making further predictions on the effects of antibiotics, and for the effects of prebiotic supplementation.

5.4 Methods

5.4.1 Model overview

In this study we have extended a multiscale model of the infant gut. The model is based on our earlier microbiota models [122, 103, 229]. The major addition in this study is the inclusion of disturbances of the microbiota. All parameters of the system are listed in table 5.2.

5.4.2 Species composition

The list of species in the model (table 5.1) is based on *in vivo* data from [3], using sheet 2 of their Table S3. We selected the 20 entries with the highest prevalence in vaginally delivered newborns. After removing two duplicate entries we selected a GEM of a species from each genus from [10]. We added GEMs of *Bifidobacterium breve* and *Bifidobacterium bifidum* to represent the diversity of *Bifidobacterium* species in the infant gut [164]. We also added a GEM of the butyrate producer *Roseburia inulinivorans*, as in our previous model [229]. *Roseburia inulinivorans*, *Eubacterium hallii*, and *Clostridium butyricum* are combined and listed as "Butyrate producers" in the visualisations.

5.4.3 Changes to GEMs

To improve the metabolic predictions of the model we applied a number of changes to the GEMs compared to the version in the AGORA database, as in our previous studies [103, 229]. No further changes were made after those in chapter 4. A full list of changed and added reactions is in table S1.

5.4.4 FBA approach

We continued to use the same FBA approach as in previous versions of the model [103, 229] and earlier chapters. This is a modified version of flux balance analysis with an enzymatic constraint [13, 100]. Each GEM is first converted to a stoichiometric matrix S. Reversible reactions are then converted to two irreversible reactions, so that flux is always greater than or equal to 0. Reactions identified in the GEM as 'exchange', 'sink', or 'demand' are allowed to take up or deposit metabolites into the environment. Each timestep, all reactions are assumed to be in internal steady state:

$$S \cdot \vec{f} = 0, \tag{5.1}$$

where $\vec{f}$ is a vector of the metabolic fluxes through each reaction in the network, in mol per time unit per population unit.

Table 5.2: Parameters of the model

Parameter	Value	Unit
Lattice side length	2	mm
Width of lattice	225	lattice sites
Height of lattice	8	lattice sites
Timestep	180	seconds
Initial populations	540	average number
New population placement probability	0.00005	per timestep per empty lattice site
Population death probability	0.0075	per timestep per population
Initial size per population	$5 \cdot 10^7$	no. of bacteria
Population size to create new population	$1 \cdot 10^{10}$	no. of bacteria
Maximum population size	$2 \cdot 10^{10}$	no. of bacteria
ATP to grow one cell	$1 \cdot 10^{-15}$	mol
Enzymatic constraint	2	µmol flux per timestep per $1 \cdot 10^{10}$ bacteria
Public goods production rate	2	µmol per nutrient per timestep per $1 \cdot 10^{10}$ bacteria
Nutrient input	211	µmol per nutrient every 60 timesteps
Mucin input	0.5	µmol per timestep
Initial oxygen	0.1	µmol per lattice site
Metabolic advection	2	mm per timestep
Diffusion of metabolites and bacteria	$6.3 \cdot 10^5$	square cm per second

Each reaction that takes up metabolites from the environment F_{in} is constrained by an upper bound F_{ub}, which represents the availability of metabolites from the environment. It is determined as follows:

$$\vec{F_{in}} \leq \vec{F}_{ub}, \tag{5.2}$$

where $\vec{F_{in}}$ is a vector of fluxes between the environment and the bacterial population. $\vec{F}_{ub}$ is a vector of upper bounds on these fluxes. $\vec{F}_{ub}$ is set dynamically at each timestep t by the spatial environment at each lattice site $\vec{x}$:

$$\vec{F}_{ub}(\vec{x}, t) = \frac{\vec{c}(\vec{x}, t)}{B(\vec{x}, t)}, \tag{5.3}$$

where $\vec{c}$ is a vector of all metabolite concentrations in mol per lattice site, $\vec{x}$ is the location and $B(\vec{x}, t)$ is the size of the local bacterial population. $\vec{F}_{ub}$ is set to 0 for any metabolite that is digested outside the cell (see section 'extracellular metabolism'). The total flux in each FBA solution is constrained by the enzymatic constraint a, in mol per time unit per population unit:

$$\sum \vec{f} \leq a. \tag{5.4}$$

Given these constraints, FBA identifies the solution that optimizes the objective function, ATP production. The solution consists of a set of input and output exchange fluxes $\vec{F_{in}}(\vec{x}, t)$ and $\vec{F_{out}}(\vec{x}, t)$, and a growth rate $g(\vec{x}, t)$. The exchange fluxes are taken as the derivatives of a set of partial-differential equations to model the exchange of metabolites with the environment. The size of the population increases proportionally to the growth rate in the FBA solution. Populations above $2 \cdot 10^{10}$ bacteria do not perform metabolism, to mimic quiescence at high densities.

Diffusion is applied to the metabolite concentrations on each lattice site at each timestep to represent mixing by colonic contractions. Metabolic diffusion is applied twice during each timestep. Each time it is applied, 14.25% of each metabolite diffuses from each lattice site to each of the four nearest neighbours. This causes a net diffusion each timestep of $6.3 \cdot 10^5$ cm^2/s. Metabolites are also added and removed by bacterial populations as a result of the FBA solutions. The change in concentration per lattice site is thus determined as follows:

$$\frac{d\vec{c}(\vec{x},t)}{dt} = \vec{F_{out}}(\vec{x},t)B(\vec{x},t) - \vec{F_{in}}(\vec{x},t)B(\vec{x},t) + \frac{D}{L^2}\sum_{\vec{i}\in \mathrm{NB}(\vec{x})}\left(\vec{c}(\vec{i},t) - \vec{c}(\vec{x},t)\right), \quad (5.5)$$

where $\vec{F_{out}}(\vec{x},t)$ is a vector of fluxes from the bacterial populations to the environment, in mol per time unit per population unit, and D is the diffusion constant, L is the lattice side length, and $NB(\vec{x})$ are the four nearest neighbours.

To represent advection all metabolites except oxygen are moved distally by one lattice site every timestep. Metabolites at the most distal column of the lattice, the end of the colon, are removed from the system at each timestep. This represents the simulated feces.

5.4.5 Nutrient input

Mucin is added each timestep in equal concentration to the lowest row of the model, to represent secreted mucin. The mucin struture we use is identified in the VMH database as MGlcn23_rl. Nutrients representing inflow from the small intestine are inserted into the first six columns of lattice sites every 60 timesteps, representing three hours. Three hours is a realistic feeding interval for newborn infants [175]. Food intake contains 211 µmol of lactose by default, a concentration in line with human milk [66], assuming 98% host uptake of carbohydrates before reaching the colon [131]. In some simulations additional lactose, GOS, or 2'-FL is added. GOS is inserted as separate fractions of DP3, DP4, or DP5 based on analysis of the composition of Vivinal-GOS [206]. 64% is DP3, 28% is DP4 and 8% is DP5. Water is provided in unlimited quantities.

5.4.6 Extracellular metabolism

Extracellular metabolism is handled through a system separate from FBA in the model. Mucins are always digested extracellularly, as are GOS chains of four or five sugars. *Bifidobacterium bifidum* also digests 2'-FL and GOS chains of length three extracellularly. The system uses the set of extracellular reactions from the GEM. Extracellularly digested oligosaccharides are excluded from FBA. Instead, the model directly applies each extracellular reaction at a rate of 2 µmol per $1 \cdot 10^{10}$ local population per timestep. This alters the set of input exchange fluxes $\vec{F_{in}}$ and

output exchange fluxes $\vec{F_{out}}$, as used in eq. 5.5. If multiple reactions can apply to a substrate, and insufficient substrate is available for each reaction to apply fully, each reaction is applied to half the remaining substrate. No substrate has more than two reactions associated with it in the model, so breakdown can never exceed the available substrate:

$$\vec{F_e}(\vec{x},t) \leq \frac{\vec{c}(\vec{x},t)}{B(\vec{x},t)}. \tag{5.6}$$

All oligosaccharide-related reactions are listed in S1 table. All mucin breakdown reactions are listed in S2 table.

5.4.7 Population dynamics

We initialize the model by giving each lattice site a population of $5 \cdot 10^7$ bacteria of a single random species at a probability of 0.3. Each timestep, each population solves the FBA problem based on its GEM, the enzymatic constraint a, its current population size $B(\vec{x},t)$ and the local concentrations of metabolites $\vec{c}(\vec{x},t)$. The outcome is applied to the environment (eq. 5.5) and the growth rate $g(\vec{x},t)$ is applied to the local population size:

$$\frac{dB(\vec{x},t)}{dt} = B(\vec{x},t)g(\vec{x},t). \tag{5.7}$$

New bacterial populations can be created in two ways. (1) each population of at least $1 \cdot 10^{10}$ bacteria creates a new population of the same species in an adjacent empty lattice site. Half the population size is transferred to the new population. (2) Each empty lattice site has a probability of 0.00005 to get a new population of $5 \cdot 10^7$ bacteria each timestep. All species have an equal probability to be selected.

Bacterial populations are mixed by swapping population contents between lattice sites during each timestep. We use an algorithm inspired by Kawasaki dynamics [176] to mix the bacterial populations. Each site is addressed in a random order, and the bacterial population size $B(\vec{x},t)$ and the GEM are swapped with a site randomly selected from the Moore neighbourhood. The swap only occurs if both the origin and destination site have not swapped in this timestep. With this mixing method the diffusion constant of the bacterial populations is $6.3 \cdot 10^5 cm^2/s$, equal to that of the metabolites. Bacterial populations at the most distal column, i.e. at the exit of the colon, are removed from the system. Populations are also removed from the system at a probability of 0.0075 per population per timestep. Disturbances are implemented

in the model by increasing the probability for a population to be removed by a factor K on days 8 and 9 of the model. We use values for K of 1.75, 2, 2.25, and 2.5. These correspond with a population approximately 81%, 91%, 97%, and 99% lower than in the undisturbed simulations immediately after the disturbance period (Fig. 5.1C).

5.4.8 Analysis

The model records the the size, species, location, and important exchange fluxes $\vec{F_{in}}(\vec{x},t)$ and $\vec{F_{out}}(\vec{x},t)$ for each population. In addition, the metabolites and nutrients leaving the system distally were recorded every timestep, and summed over every 60 timesteps for visualisations. Euclidean distance between relative abundances was calculated as follows:

$$d(\vec{p},\vec{q}) = \sqrt{\sum_{i=1}^{n}(p_i - q_i)^2}, \tag{5.8}$$

where d is the distance between the vectors $\vec{p}$ and $\vec{q}$. $\vec{p}$ and $\vec{q}$ are vectors of the bacterial abundance, either grouped by species or as in table 5.1. This distance metric indicates how far away each set of simulations is from the undisturbed endpoint.

5.4.9 Implementation details

The model is implemented in C++ 11 with libSBML 5.18.0 for C++ to load GEMs and the GNU Linear Programming Kit 4.65 (GLPK) to solve the FBA problems. Random numbers were generated with Knuth's subtractive random number generator algorithm [256]. Diffusion of metabolites was implemented using the Forward Euler method. The model is based on our own earlier models of the gut microbiota [122, 103, 229]. GEMs are sourced from the May 2019 update of AGORA, from the Virtual Metabolic Human Project website (vmh.life). We used Python 3.6 to extract thermodynamic data from the eQuilibrator API (December 2018 update) [173]. All p-values were calculated with R 4.2.2. Unless noted otherwise p-values were calculated using the Mann-Whitney test ('wilcox.test') from the 'stats' package. ANOVA tests used the 'aov' function from the 'stats' package. Principal component analysis was done with the 'prcomp' function from the 'stats' package. Shannon diversity was calculated using the function 'diversity' from the 'vegan' package. Sheldon's index was calculated using the 'sheldon' function from the 'seqtime' package [273]. Model

screenshots were made using the libpng16 and pngwriter libraries. Other visualisations were performed with R 4.2.2. Raincloud visualisations used a modified version of the Raincloud plots library for R [216].

5.5 Supplemental material

Available from
`drive.google.com/drive/folders/11pW77mica7ugorC0Gg8MwCaaniS9PWrz`

S1 Table

S1table.csv
A table of changes made to the AGORA models as a .csv file.

S2 Table

S2table.csv
A table of mucin reactions used for public goods metabolism as a .csv file.

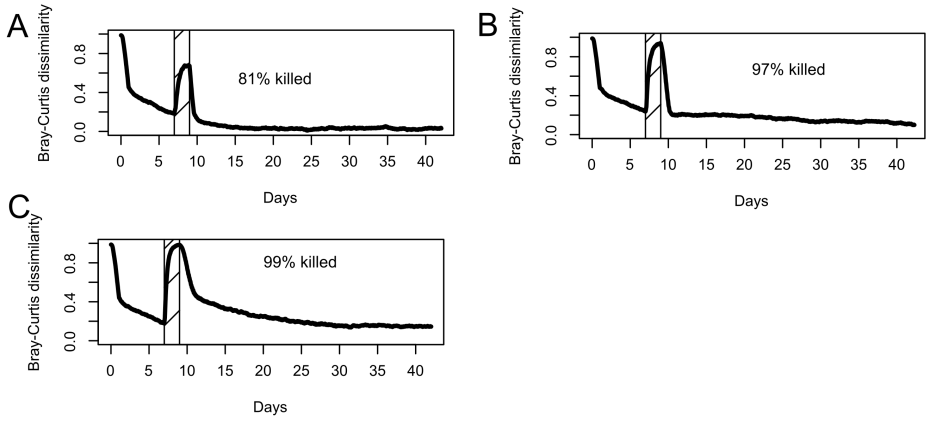

S1 Figure

(A-C) Bray-Curtis dissimilarity between the mean relative abundance per species grouped as in table 5.1 of the conditions that killed 81%, 97%, and 99%, compared to the mean relative abundance of the undisturbed simulations at day 42 (timestep 20160). Striped area indicates the duration of the disturbance. n=30 per condition.

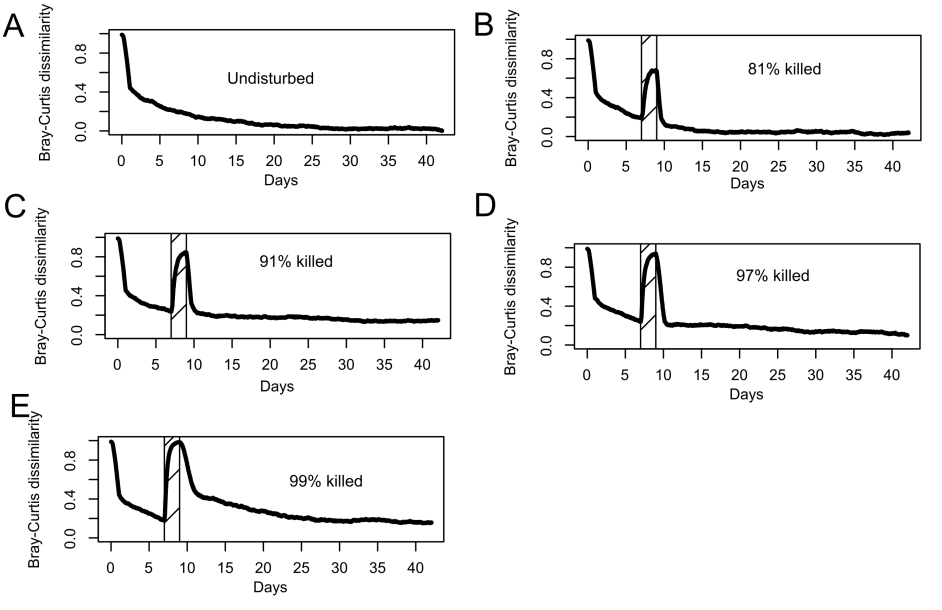

S2 Figure

(A-E) Bray-Curtis dissimilarity between the mean relative abundance per species (ungrouped) of each condition of Fig. 5.2 compared to the mean relative abundance per species (ungrouped) of the undisturbed simulations at day 42 (timestep 20160). Striped area indicates the duration of the disturbance. n=30 per condition.

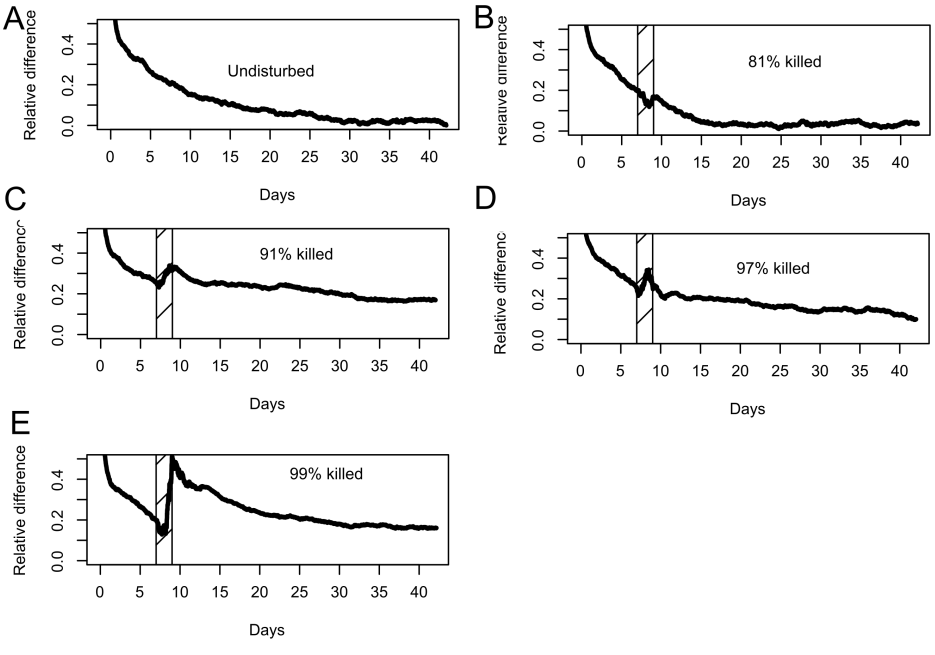

S3 Figure

(A-E) Euclidean distance between the mean relative abundance per species grouped as in table 5.1 of the undisturbed conditions and the conditions that killed 81%, 91%, 97%, and 99%, compared to the mean relative abundance of the undisturbed simulations at day 42 (timestep 20160). Striped area indicates the duration of the disturbance. n=30 per condition.

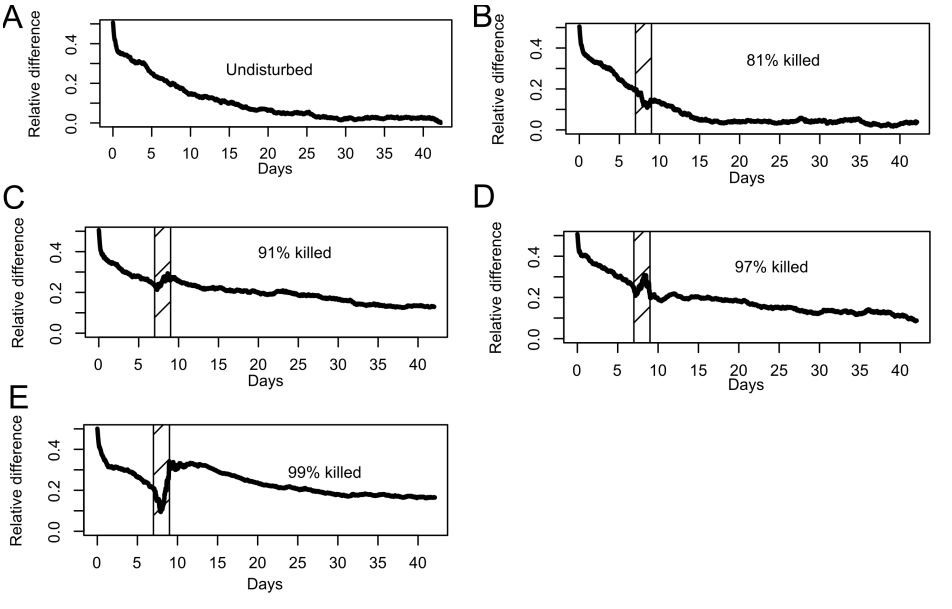

S4 Figure

(A-E) Euclidean distance between the mean relative abundance per species (ungrouped) of each condition compared to the mean relative abundance per species (ungrouped) of the undisturbed simulations at day 42 (timestep 20160). Striped area indicates the duration of the disturbance. n=30 per condition.

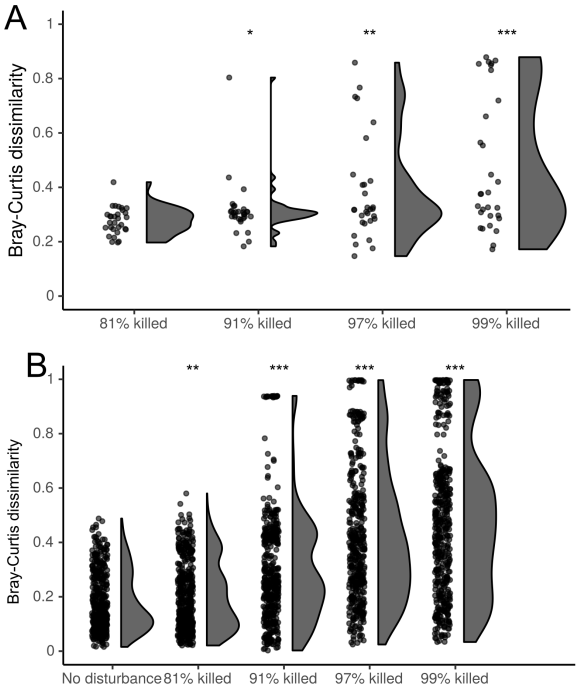

S5 Figure

(A) Bray-Curtis dissimilarity by simulation between the mean relative abundance per species (ungrouped) of each condition in Fig. 1D at day 42 (timestep 20160), compared to the mean relative abundance of the undisturbed simulations at day 42. n = 30 per condition (B) Bray-Curtis dissimilarity of the grouped abundance at day 42 (timestep 20160) of each simulation compared to each other simulation within each condition. n=30 per condition, leading to 450 unique comparisons for each condition. NS: Not significant, *: $p<0.05$, **:$p<0.01$, ***:$p<0.001$

5.5. Supplemental material

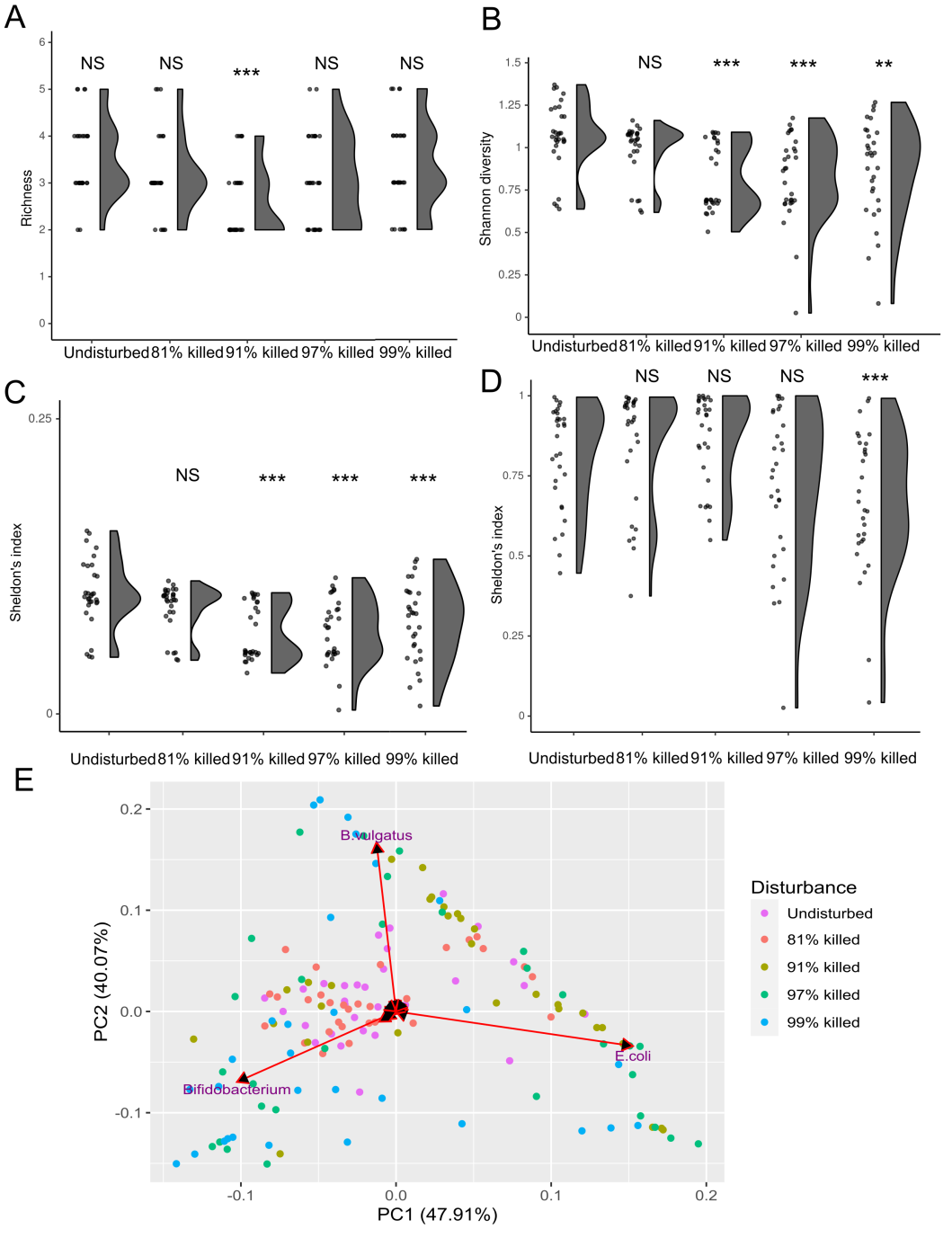

S6 Figure

(A) Richness for all simulations of Fig.5.2 in each condition at day 42 (timestep 20160), with a threshold of 10^{10} bacteria for each species to be counted. (B) Shannon diversity for all simulations of Fig.5.2 in each condition at day 42 (timestep 20160), with a threshold of 10^{10} bacteria for each species to be counted. (C) Sheldon's index for all simulations of Fig.5.2 at day 42 (timestep 20160) (D) Sheldon's index for all simulations of Fig.5.2 at day 42 (timestep 20160), where we set the abundance of each species at 0 if it was below 10^{10} bacteria. (E) Principal component analysis for all simulations of Fig.5.2 at day 42, using the abundance of each bacterial genus. Arrows displayed for each genus, labels included for the largest three. NS: Not significant, *: $p<0.05$, **:$p<0.01$, ***:$p<0.001$

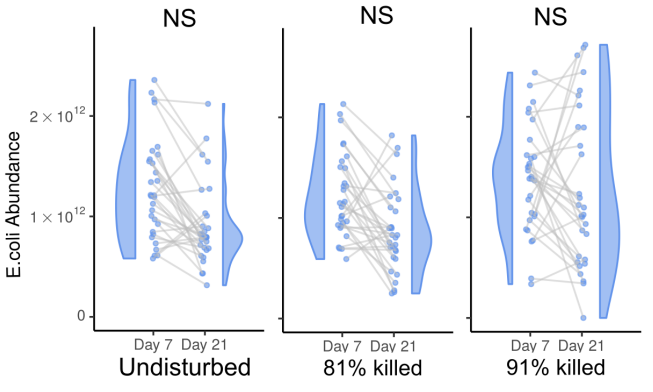

S7 Figure

Absolute abundance of *E. coli* per simulation at the end of day 7 and day 21 for the first three conditions of Fig. 1D. Points from the same simulation are connected with a line. Spearman correlation between day 7 and day 21 indicated where significant. n=30 per condition. NS= Not significant.

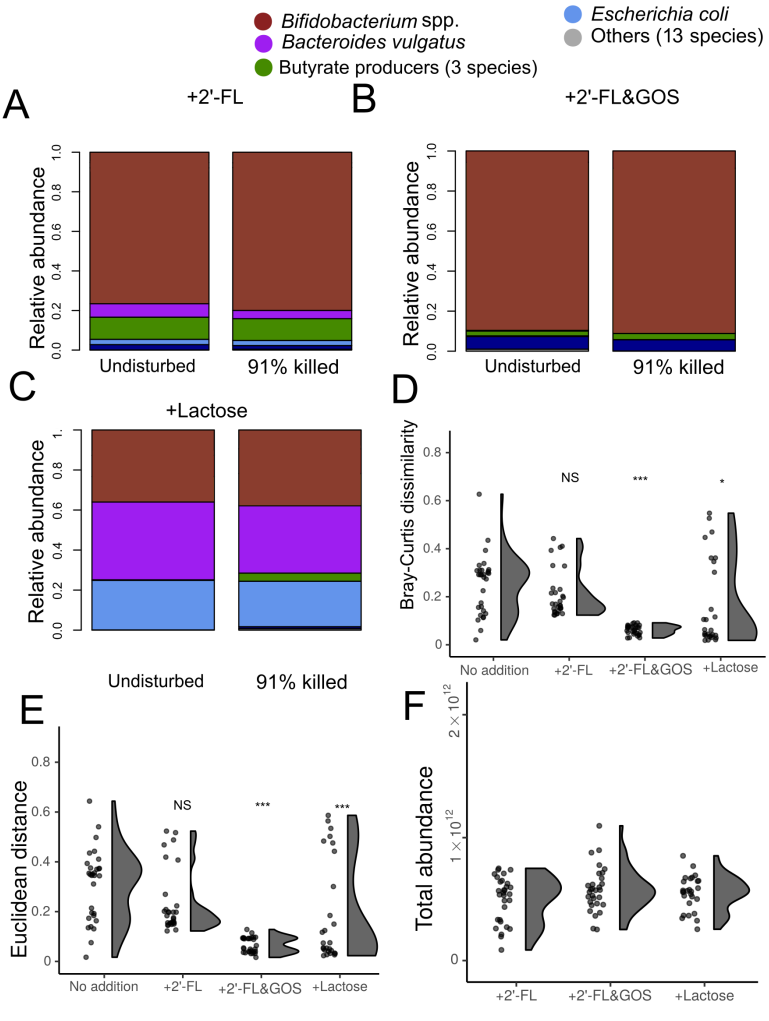
Bifidobacterium spp.
Bacteroides vulgatus
Butyrate producers (3 species)
Escherichia coli
Others (13 species)
A
+2'-FL
B
+2'-FL&GOS
Relative abundance
Undisturbed
91% killed
C
+Lactose
D
Bray-Curtis dissimilarity
NS
***
*
No addition
+2'-FL
+2'-FL&GOS
+Lactose
E
Euclidean distance
F
Total abundance

S8 Figure

(A-C) Relative abundance of bacterial species on day 42 without disturbance or with the death rate increased on the simulated day 8 and 9, with the addition of either 211 µmol lactose and 211 µmol FL per 60 timesteps, 211 µmol lactose, 42 µmol 2FL and 169 µmol GOS, or 422 µmol lactose. n=30 per condition. (D) Bray-Curtis dissimilarity by simulation between the mean relative abundance grouped as in table 5.1, at day 42 (timestep 20160) and the mean relative abundance grouped in the same way of the corresponding undisturbed simulations at day 42. All use the disturbance that killed 91%. n=30 per condition (E) Euclidean distance by simulation between the mean relative abundance grouped as in table 5.1, at day 42 (timestep 20160), compared to the mean relative abundance grouped in the same way of the corresponding undisturbed simulations at day 42. All use the disturbance that killed 91%. n=30 per condition (F) Total bacterial abundance at the start of day 10 per condition in the simulations with disturbance of A-C. n=30 per condition. NS: Not significant, *: $p<0.05$, **:$p<0.01$, ***:$p<0.001$

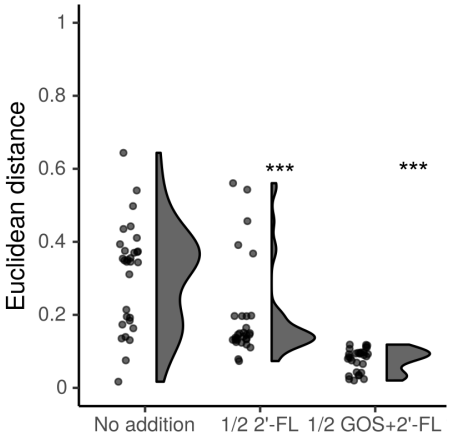

S9 Figure

Euclidean distance by simulation between the mean relative abundance per species grouped as in table 5.1 of each condition in Fig. 5.4A at day 42 (timestep 20160), compared to the mean relative abundance of the undisturbed simulations at day 42. n = 30 per condition. NS: Not significant, *: $p<0.05$, **:$p<0.01$, ***:$p<0.001$

5.6 Contributions

J.M.W.G., and R.M.H.M acquired funding. D.M.V., J.M.W.G., E.L., and R.M.H.M. conceived and planned the simulations. D.M.V. wrote software used for the simulations. D.M.V. performed the simulations and analyzed the data. E.L., J.M.W.G., and R.M.H.M contributed to the interpretation of the results. J.M.W.G., and R.M.H.M. supervised the project. D.M.V. drafted the manuscript. D.M.V., E.L., J.M.W.G. and R.M.H.M. revised and edited the manuscript.

5.7 Acknowledgments

This study was financially supported by FrieslandCampina. E.L., and J.M.W.G. are currently employed by FrieslandCampina. This work was performed using the ALICE compute resources provided by Leiden University.